Research Article J. Electrochem. Sci. Technol., 2018, 9(3), 229-237

Journal of Electrochemical Science and Technology
jecst.org

Free-standing Three Dimensional Graphene Incorporated with Gold Nanoparticles as Novel Binder-free Electrochemical Sensor for Enhanced Glucose Detection

Quoc Bao Bui[1], Dang Mao Nguyen[2]*, Thi Mai Loan Nguyen[3], Lee Ku Kwac[4], Hong Gun Kim[4], Sang Cheol Ko[4], and Hun Jeong[4]*

[1]*Sustainable Developments in Civil Engineering Research Group, Faculty of Civil Engineering, Ton Duc Thang University, Ho Chi Minh City, Vietnam*
[2]*Department of Polymer and Composite Materials, Faculty of Material Science, University of Science, Vietnam National University Ho Chi Minh city (VNU), Vietnam*
[3]*The National Centre of Drug Information and Adverse Drug Reaction Monitoring, Hanoi University of Pharmacy, Hanoi, Vietnam*
[4]*Institute of Carbon Technology, Jeonju University, Jeonju, Jeonbuk 55069, Republic of Korea*

ABSTRACT

The electrochemical sensing performance of metal-graphene hybrid based sensor may be significantly decreased due to the dissolution and aggregation of metal catalyst during operation. For the first time, we developed a novel large-area high quality three dimensional graphene foam-incorporated gold nanoparticles (3D-GF@Au) via chemical vapor deposition method and employed as free-standing electrocatalysis for non-enzymatic electrochemical glucose detection. 3D-GF@Au based sensor is capable to detect glucose with a wide linear detection range of 2.5 μM to 11.6 mM, remarkable low detection limit of 1 μM, high selectivity, and good stability. This was resulted from enhanced electrochemical active sites and charge transfer possibility due to the stable and uniform distribution of Au NPs along with the enhanced interactions between Au and GF. The obtained results indicated that 3D-GF@Au hybrid can be expected as a high quality candidate for non-enzymatic glucose sensor application.

Keywords : Gold nanoparticles, Graphene foam, Nanohybrid, Catalyst, Glucose sensor

Received : 16 May 2018, Accepted : 4 July 2018

1. Introduction

Recent years have perceived tremendous evolution in the development and use of nanomaterials towards biological and biomedical applications. Among these nanomaterials, graphene (GR), a two-dimensional monolayer of sp^2-hybridized carbon atoms, has attracted enormous interest due to its extraordinary properties [1,2]. In particular, two and three dimensional (3D) metal-graphene hybrids have demonstrated to provide new advances in various fields, such as field-effect transistors, biological/chemical sensors, energy applications, gas barrier, and transparent conductors [3-6]. Although many promising applications have been demonstrated, a huge challenge and need still remains for the efficient use of graphene's large specific surface area and extraordinary electrical, chemical, and mechanical properties. The hybrid based on chemically synthesized graphene (GR), such as GO and rGO with metal catalysts are extensively employed due to the ease of synthesis, low cost, and large-scale production [5-10]. However, abundant defects and chemical moieties created on such GR structures during the synthesis make a reduction of electric conductivity as well as high intersheet contact resistance. In addition,

*E-mail address: ndmao@hcmus.edu.vn(Dang Mao Nguyen), feerself@jj.ac.kr(Hun Jeong)

DOI: https://doi.org/10.5229/JECST.2018.9.3.229

aggregation and restacking between individual GR sheets also greatly compromise its intrinsic specific surface area. As a result, the physicochemical and electrochemical properties of hybrid materials can be significantly reduced. Recently, growth of GR using chemical vapor deposition (CVD) approach demonstrated high potential to improve the aforementioned problems that currently plague the performance of GR hybrids. As compared to two dimensional GR materials, three-dimensional GR foam (3D-GF) can provide more advantages, including porous and interconnected network, high electrical conductivity, large accessible surface area, and excellent mechanical and thermal stability. Due to their unique structures and outstanding properties, 3D-GF is really suitable as a high quality platform for attaching active metal material for electrochemical applications. In this regard, Au-based nanostructures have been emerging is an excellent electrocatalyst with a series of fascinating properties such as optical properties, electrochemical and electrocatalytic properties [11-13]. Thus, Au nanostructures have been extensively applied for different applications, such as the oxidation of CO, the water gas shift reaction, alcohol electrooxidation, glucose oxidation [13-15]. In particular, Au-based nanostructures have demonstrated great potentials in the applications of electrochemical sensors due to high catalytic behavior, high active surface area, good biocompatibility, and physicochemical stability [16-18]. By combining the merits of 3D-GF with the high chemical/electrochemical activities of Au NPs, the formation of 3D-GF@Au-based hybrid can be great promise as high-performance electrode materials in sensor applications. However, low uniformity, aggregation, and dissolution of active Au metal are still the critical issues due to low interactions between metal and the hydrophobic GR. In efforts to solve these issues, some approaches, such as acid treatment, oxygen plasma treatment, and heteroatom doping process, have been employed to enhance hydrophilic feature of 3D-GF [19-22]. However, the complicated procedure, high cost, and low efficiency rather limited their applications. To address this mentioned issues, we developed a novel approach to synthesize 3D-GF incorporated with highly uniform Au NPs via CVD method. By this way, it was demonstrated that the formation of such nanostructure can facilitate the well dispersion state of the Au NPs and speed up the charge transfer, then exhibiting an outstanding electrocatalytic activity, long-term stability in electrochemical glucose sensing applications.

2. Experimental

2.1 Materials

Hydrogen tetrachloroaurate ($HAuCl_4.3H_2O$), ascorbic acid (AA), uric acid (UA), ethanol, glucose, dopamine (DA), and poly(methyl methacrylate) (PMMA) were purchased from Aldrich Co. (USA). Sodium hydroxide (NaOH), sulfuric acid (H_2SO_4), hydrochloric acid (HCl), potassium chloride (KCl), acetone, acetic acid, and ethanol were purchased from Samchun Pure Chemical Co. (Korea). Nickel foam, provided by Alfa Aesar Co. (USA), was used as the substrate to grow 3D-GF. Argon, hydrogen, nitrogen, and methane gas were used as carrier, reducing and carbon source gas, respectively.

2.2 Synthesis of 3D-GF@Au hybrid

Prior to growth of the 3D-GF@Au hybrid, Ni foam (1 cm × 2 cm) was cleaned by dipping in each solvent of acetone, ethanol, acetic acid, and deionized water for 10 min, respectively. After Ni foam was dried by N_2 gas, it was deposited with Au NPs through immersing in 1 mM $HAuCl_4$ solution for various time periods, such as 3, 5, and 7 min. In this regard, the spontaneous oxidation-reduction reaction between Ni surface and Au^{3+} ions happened due to the smaller reduction potential of Ni surface (-0.25 V) as compared to Au^{3+} ions (+1.4 V), thereby resulting in Au nanoparticles (NPs) deposited on surface of Ni foam [23]. Varying the deposition time with 3, 5, and 7 min can lead to the change of deposited amount as well as structure of Au NPs on Ni surface; which influence on the electrochemical performance of final product. Au deposited Ni (Au/Ni) foam were dried in nitrogen environment at room temperature and then was used as substrate for growing GF. In a specific procedure, Au/Ni foam was placed at the center of a quartz tube and was heated to 1000°C at a 50°C/min heating rate under atmospheric pressure of a gas mixture H_2 (35 sccm) and Ar (1000 sccm). After stabilizing for 20 min, GR was grown by flowing CH_4 (50 sccm) into CVD reactor for 10 min, then followed by rapidly cooling to the room temperature under Ar flow (1000 sccm). The sample was then coated with a thin PMMA layer by dipping in PMMA solution (6 wt%) for 30 s and was dried at

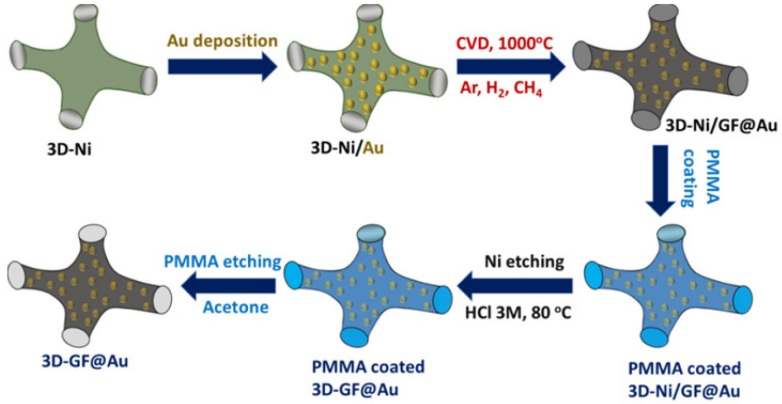

Scheme 1. Schematic illustration of 3D-GF@Au hybrid fabrication.

120°C for 3 min. The Ni foam was etched away using 3 M HCl solution at 80°C for 24 h. Finally, PMMA was removed by acetone at 55°C for 3 h to leave the free-standing 3D-GF@Au sample. According to deposition time, the final products were named as 3D-GF@Au-3, 3D-GF@Au-5, and 3D-GF@Au-7. A 3D-GF sample without depositing Au NPs was also synthesized as a comparison by similar procedure.

2.3 General characterization

Raman characterization was performed using a Nanofinder 30 (Tokyo Instruments Co., Osaka, Japan). Scanning electron microscopy (SEM) image and energy-dispersive X-ray spectroscopy (EDS) were carried out on a JSM-6701F (JEOL, Japan). X-ray photoelectron spectroscopy (XPS) was used to investigate elemental composition through a Theta Probe instrument (Thermo Fisher Scientific Inc., USA).

Electrochemical characterizations were performed in a three-electrode electrochemical cell using an Electrochemical Workstation ZIVE SP2 (WonATech Co., South Korea). The platinum wire and a saturated Ag/AgCl electrode were used as the counter electrode and the reference electrode, respectively, for electrochemical measurements. 3D-GF@Au pieces (1 cm × 1 cm) were kept by a metal clamp to be used as working electrodes. Cyclic voltammetry (CV), electrochemical impedance spectroscopy (EIS), and amperometric measurements were carried out to investigate electrochemical properties of materials. The 0.1 M NaOH and 0.5 M H_2SO_4 solution were used as electrolytes for electrochemical characterizations at 25°C.

3. Results and Discussion

The FE-SEM analysis was performed to characterized surface properties of materials. After the Ni template was etched, the GR film fully interconnected throughout the entire 3D foam without collapsing phenomenon (Fig. 1a). High magnification SEM image showed that GR was uniformly formed under a thick multilayered structure. In addition, a numerous large number of interdomain defects were clearly observed (Figs. 1b and c). In the case of 3D-GF@Au hybrids, SEM image indicated that entire 3D framework was wrapped with GR structure. The presence of Au NPs was observed with the uniform distribution and penetration to the inner of the GF networks. The mean size of Au NPs in 3D-GF@Au-3 was found to be around 20-25 nm (Figs. 1d and e), which is relatively similar to particle size of Au in 3D-GF@Au-5 (Figs. 1g and h), but significantly smaller than that of 3D-GF@Au-7 (Figs. 1g and k). In addition, the density of Au NPs in hybrids increased with the increase of deposition time. In this regard, the content of Au in hybrid was found to be around 9.7 wt%, 19.8 wt%, and 30.1 wt% for 3D-GF@Au-3, 3D-GF@Au-5, and 3D-GF@Au-7, respectively. The formation of continuous 3D GR network with good dispersion of Au NPs can provide an effective pathway for charge transfer, more channels and active surface area to accelerate the interfacial reaction [24]. In addition, the penetration of Au NPs into GR struc-

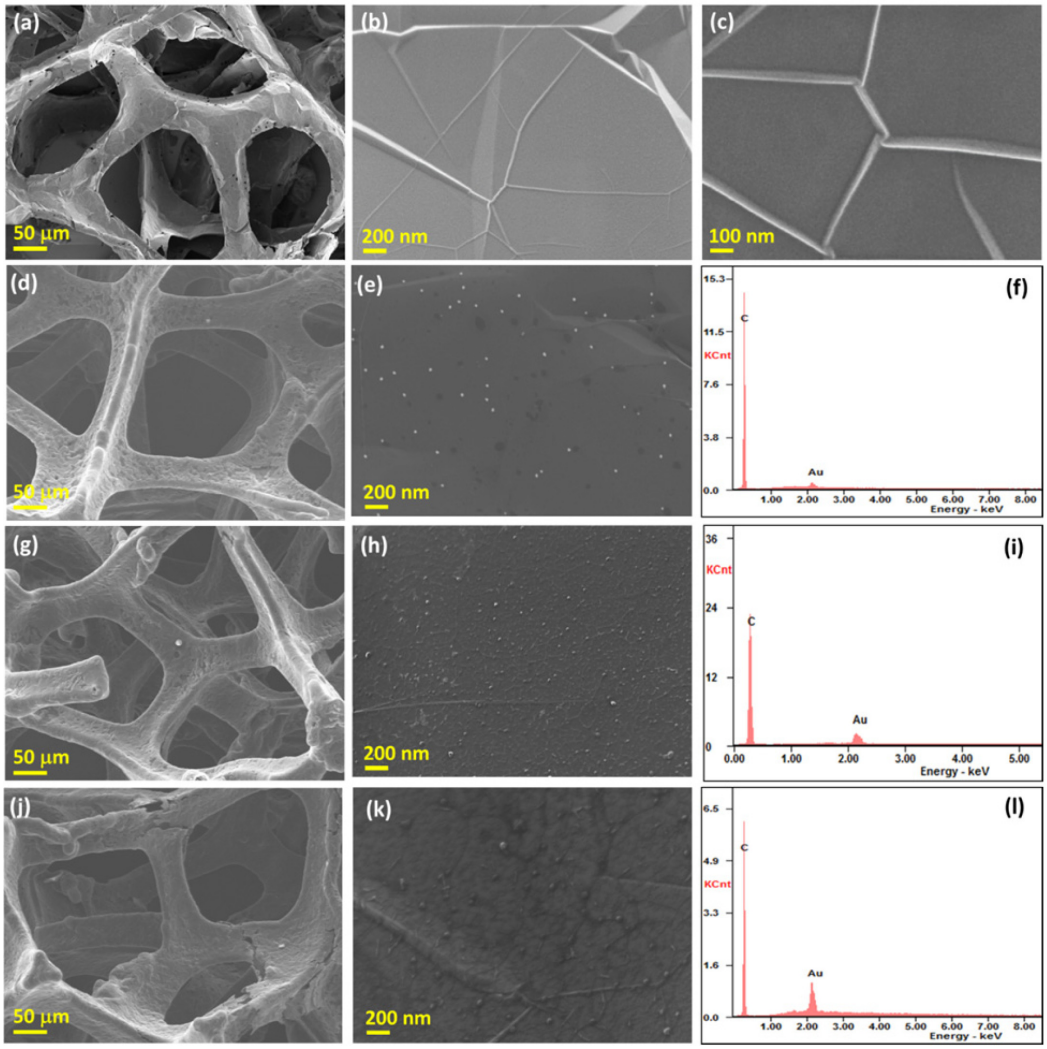

Figure 1. (a-c) FE-SEM images of 3D-GF; (d and e) FE-SEM images and (f) EDS result of 3D-GF@Au-3; (g and h) FE-SEM images and (i) EDS result of 3D-GF@Au-5; (j and k) FE-SEM images and (l) EDS result of 3D-GF@Au-7 materials.

ture also significantly reduced contact resistance and enhanced the cycle stability of electrode suitable for electrochemical sensing applications.

Raman spectroscopy is an efficient technique to investigate physical characteristic of GR-based materials (Fig. 2a). The average layer number and crystalline quality of the 3D-GF can be easily predicted from the 2D/G and D/G peaks ratios. It is worth noting that the 3D-GF delivered the 2D/G peak ratios of 0.64, agreeing with characteristic of multilayered structure [25], which is suitable to work as a stable template to load active materials for electrochemical reactions [26,27]. The value of the D/G peaks ratio was found to be 0.12, indicating that such multilayered graphene has crystal structure without significant defects [28]. Meanwhile, the 3D-GF@Au-3, 3D-GF@Au-5, and 3D-GF@Au-7 materials showed that the growth of GR on Au deposited Ni foam can lead to an increase of defect number of the obtained GR structure, as similarly seen in previous reports [2,23,29]. The high value of 2D/G peaks ratio was found around 0.58, 1.24, and 1.43 for the 3D-GF@Au-3, 3D-GF@Au-5, and 3D-GF@Au-7, respectively, corresponding to the high disorder of

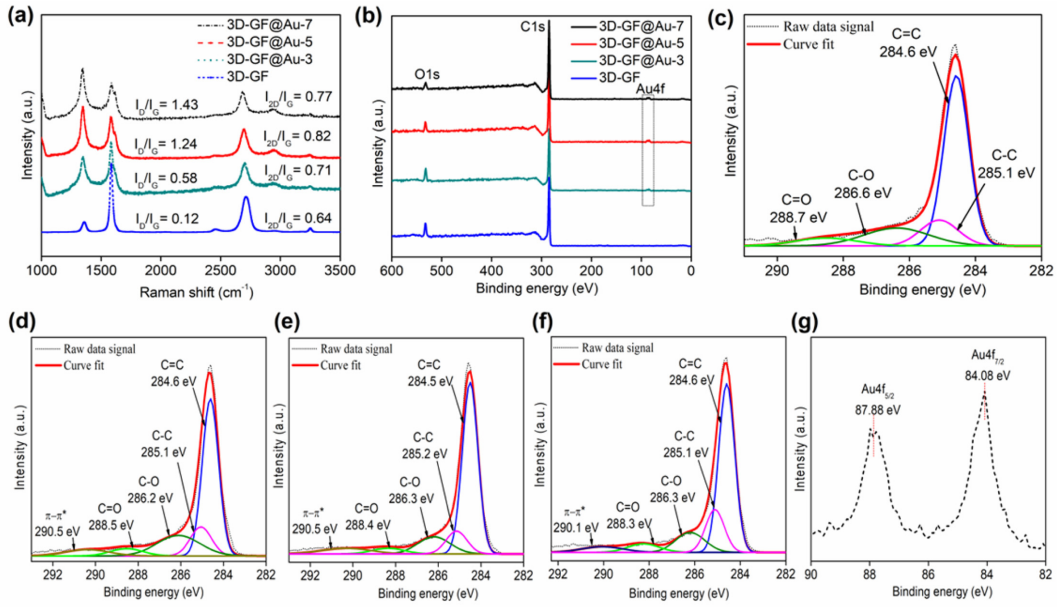

Fig. 2. (a) Raman spectra and (b) XPS spectra of 3D-GF, 3D-GF@Au-3, 3D-GF@Au-5 and 3D-GF@Au-7 materials; High resolution C1s XPS spectrum of (c) 3D-GF, (d) 3D-GF@Au-3, (e) 3D-GF@Au-5, and (f) 3D-GF@Au-7 materials; (g) High resolution XPS spectrum for Au4f in 3D-GF@Au-5 material.

the GR structure. This obviously indicated the creation of new active sites on the GR surface induced by Au NPs as compared to 3D-GF [2,23,29].

The chemical bonding on the material surface was investigated by XPS technique. Fig. 2b shows the survey spectra of 3D-GF and 3D-GF@Au hybrids with presence of C1s, O1s, and Au4f peaks. The presence of small intensity for O1s in both materials may be resulted from some polymer residues after transferring process [30]. In addition, it may be the presence of significant functional groups containing oxygen adsorbed on graphene structure due to the increase of its defect amount [31,32]. The deconvoluted C1s spectrum for 3D-GF@Au-3 (Fig. 2d), 3D-GF@Au-5 (Fig. 2e), and 3D-GF@Au-7 (Fig. 2f) showed different peaks that correspond to C=C, C-C, C-O, C=O, and π-π* bonding, respectively. The percentage of C=C species in the 3D-GF@Au-3, 3D-GF@Au -5, and 3D-GF@Au -7 hybrid was calculated to be around 55.8%, 56.2%, and 58.6%, which are significantly reduced as compared to that of 3D-GF sample (62%) (Fig. 2c), indicating the increase of defect amount in hybrid structures. The high resolution XPS spectrum of Au4f in 3D-GF@Au-5 showed two peaks at 84.08 and 87.88 eV consistent with Au4f7/2 and Au4f5/2, respectively (Fig. 2g). Interestingly, the Au4f peaks of Au in such hybrid downshifted to lower binding energy as compared to that of a pure Au sample [29,33], implying high interactions between Au NPs and GF.

The CV measurements were applied to determine the electrochemical active surface area (ECSA) of Au NPs in the modified electrodes. The ECSA of Au NPs can be evaluated from the charge measured under the reduction peak of Au oxides in 0.5 M H_2SO_4. Fig. 3a showed a strong peak at around 0.9 V from the reverse scan, corresponding to the reduction reaction of Au oxides. It can be seen that the integrated area of peak for 3D-GF@Au-5 was much larger than that of during the cathodic scan was used for ECSA calculations as discussed above. The charge associated with desorption of oxide in case of Au oxides was reported to be 390 μC·cm^{-2} [34]. Using this data, ECSA for Au NPs in the hybrid was calculated to be 0.025, 0.077, 0.073 cm^2 for 3D-GF@Au-3, 3D-GF@Au-5, 3D-GF@Au-7, respectively, indicating better ECSA value of Au NPs in 3D-GF@Au-5. In another aspect, the charge transfer rate of electrodes was also investigated. The better charge transfer ability was observed for the 3D-

GF@Au-5 (~68 Ω) as compared to 3D-GF (~112 Ω), 3D-GF@Au-3 (~74.8 Ω), and 3D-GF@Au-7 (~98 Ω), further implying excellent properties of such materials for electrochemical sensing applications (Fig. 3b). Due to the enhanced electroactive surface area of Au NPs and lower charge transfer resistance as compared to other hybrids, the 3D-GF@Au-5 was applied for further experiments

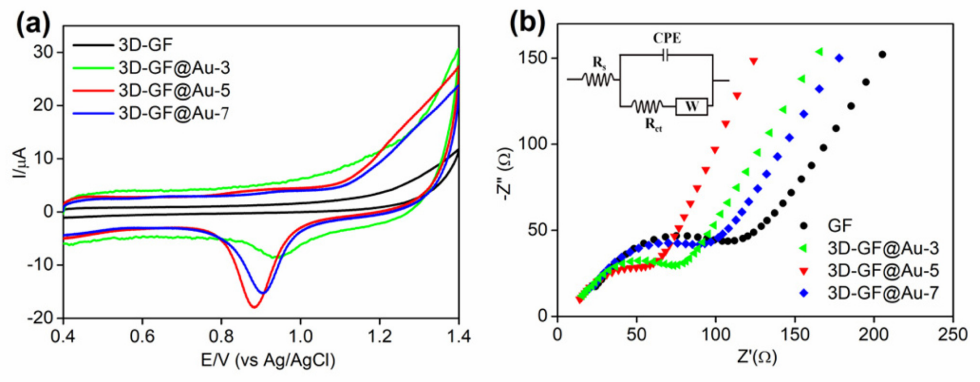

Fig. 3. (a) CV curves and (b) EIS of different materials: 3D-GF, 3D-GF@Au-3, 3D-GF@Au-5, and 3D-GF@Au-7 material.

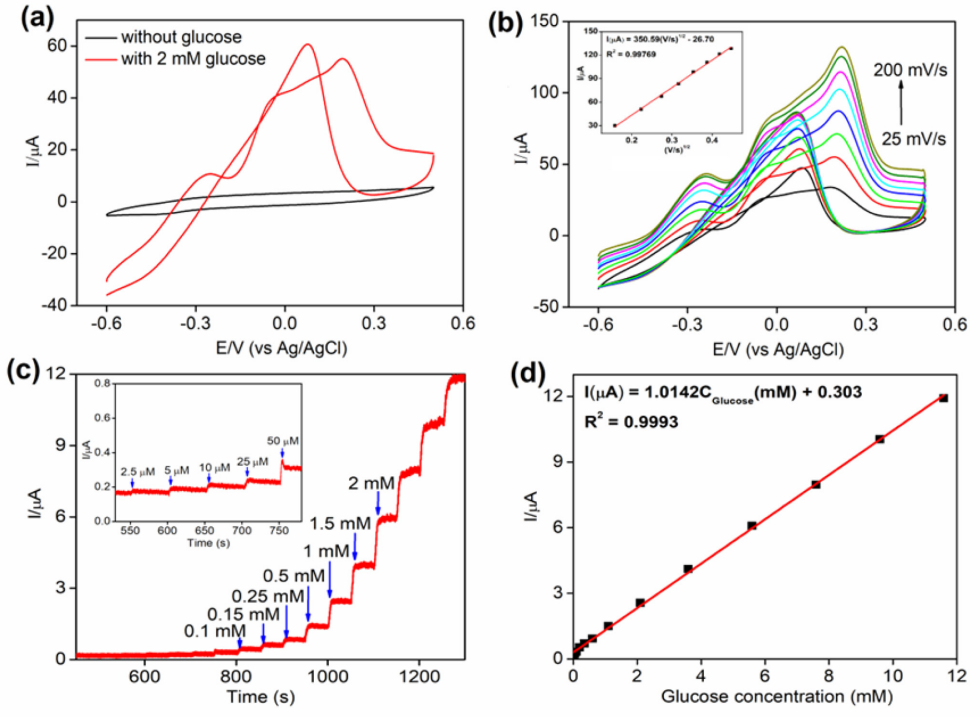

Fig. 4. (a) CVs of glucose oxidation on the 3D-GF@Au-5 electrode in 0.1 M NaOH containing 2 mM glucose at a scan rate 50 mV/s, (b) CVs of 3D-GF@Au-5 electrode at various scan rates (Inset: peak current *vs* square root of scan rate), (c) amperometric (i-t) results of the 3D-GF@Au-5 electrode according to the addition of glucose at 0.0 V, (d) plots of glucose concentration *vs* current.

Table 1. The glucose detection of the proposed sensor as compared to previous reports.

Electrode	Technique	Potential (V)	LOD (mM)	Linear range (mM)	References
AuNWs network film	Amperometry	0	0.05	0.05-15	[36]
Au-FLG	Amperometry	0	0.001	0.006-28.5	[23]
Nanoporous PtAu	Amperometry	0.6	0.0005	0.2-5.4	[37]
CQDs/octahedral Cu_2O	Amperometry	0.6	0.0084	0.02-4.3	[7]
Cu_2O/GR	Amperometry	0.6	0.0033	0.3-3.3	[38]
Nanoporous Pt	Amperometry	0.4	0.8	1-10	[39]
Au-MWCNTs-CS	Amperometry	0.2	0.0005	0.001-1.0	[40]
Ni-MoS_2/rGO	Amperometry	0.55	0.0027	0.005-8.2	[41]
3D-GF@Au-5	Amperometry	0.0	0.001	0.0025-11.6	This work

towards glucose detection.

The electrochemical oxidation of glucose at surface of 3D-GF@Au-5 electrode was initially evaluated by CV measurement in 0.1 M NaOH at a scan rate of 50 mV/s. The CVs showed no electrochemical peak current with the absence of glucose (Fig. 4a). Whereas, there were well-defined oxidation peaks in the presence of 2 mM glucose, indicating an effective response to glucose, due to the conversion of glucose to glucolonic acid [35]. In the forward scan, the oxidation peaks appearing at -0.25 V and +0.192 V were associated with the oxidation procedures in which glucose convert to gluconolactone and then gluconolactone oxidation, respectively. The reaction kinetics of glucose oxidation at the 3D-GF@Au-5 surface was evaluated by varying the potential scan rate from 25 to 200 mV/s (Fig. 4b). It can be seen that the peak current of the glucose oxidation regularly increased when scan rate was increased. The plot of peak current against square root of scan rate was linear consistent with a correlation coefficient of 0.99769 (inset in Fig. 4b), implying that the reaction kinetics of glucose oxidation at such electrode obeyed to a diffusion-controlled route.

In order to further investigate glucose detection, amperometric technique was applied to measure current responses of electrodes according to successive additions of glucose (Fig. 4c). As discussed by previous report, the amperometric measurements were operated at the applied potential of 0.0 V, which was demonstrated to provide adequate sensitivity and selectivity for the glucose detection [23]. The amperometric results showed linear detection range from 2.5 μM to 11.6 mM consistent with the linear regression equations of $I(\mu A) = 1.0142C_{glucose}(mM) + 0.303$ and a correlation coefficient of 0.9993 (Fig. 4d). The limit of detection (LOD) was found to be 1 μM (signal/noise ~3) (Fig. 5a). The sensing performance of the 3D-GF@Au-5 electrode was compared with early reported glucose sensors, and the results were shown in Table 1.

Selectivity is also an important factor for the practical application of non-enzymatic glucose sensors. The effect of various interferents on the glucose detection was evaluated by amperometric measurements. Fig. 5b shows the current responses of glucose (1 mM), KCl (0.1 M), AA (0.05 mM), UA (0.05 mM) and DA (0.005 mM) at 3D-GF@Au-5 electrode. The concentration of such interferents reaches to their real level as compared to glucose in human blood. The 3D-GF@Au-5 electrode exhibited good anti-interference performance toward KCl, AA, UA, and DA, suggesting the proposed sensor can nonenzymatic detect glucose at 0.0 V with low effect of interference. In another regard, the good performance of a biosensor requires not only a high catalyst activity, but also good stability for the prolonged working time. Therefore, the stability test of our sensor was carried out by amperometric and CV measurement. Fig. 5c showed that the current intensity with the injection of 1 mM glucose is stable with 5% loss after running time of 600 s. The stability of the 3D-GF@Au-5 electrode was also evaluated under many CV cycles in 0.1 M NaOH solution containing 2 mM glucose. It was found that such electrode displayed good stability, consistent with 90.02% retention of

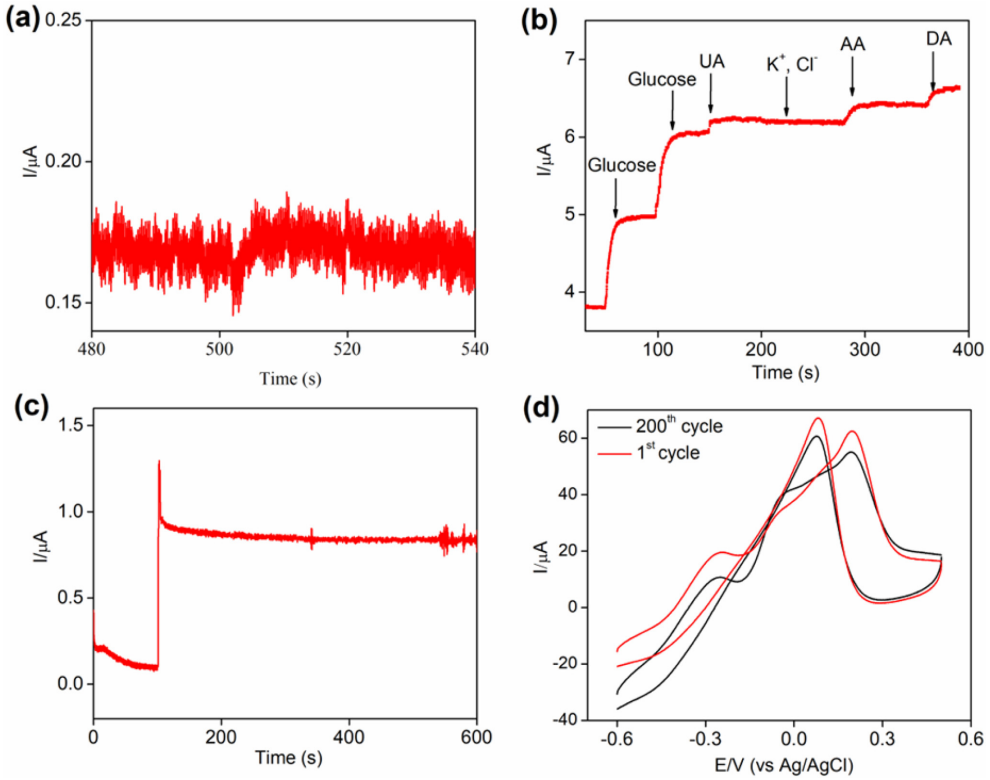

Fig. 5. (a) Amperometric response of the 3D-GF@Au-5 electrode with addition of 1 mM glucose, (b) The anti-interference ability of the proposed sensor, (c) Amperometric stability of the 3D-GF@Au-5 electrode after 600 s, (d) CV stability of the 3D-GF@Au-5 electrode after 200 cycles.

peak current for glucose oxidation after 200 cycles (Fig. 5d). The results indicate that the developed sensor not only had good sensitivity but also good selectivity and stability, thereby being highly applicable for glucose detection.

4. Conclusions

We successfully developed a novel hybrid based on GF and Au NPs via CVD approach and applied as non-enzymatic glucose sensor. SEM and TEM characterizations indicated that the Au NPs were homogeneously incorporated in the GR structure, leading to enhancement of interactions between GF and Au NPs. The electrochemical measurements demonstrated the good electrocatalytic performance of 3D-GF@Au-5 hybrid towards glucose detection with wide linear detection range of 2.5 μM-11.6 mM and low LOD of 1 μM. Furthermore, the 3D-GF@Au-5 based sensor displayed good selectivity without significant interference from of AA, DA, UA, K^+, and Cl^- together with long-term stability. The obtained results imply that the 3D-GF@Au-5 based sensor can be a prospective candidate for a potential non-enzymatic glucose sensor in real applications.

Acknowledgement

Authors would like to acknowledge support from the Basic Science Research Program (2017R1D1A1B03028413) and (2016R1A6A1A03012069) through the National Research Foundation (NRF) funded by the Ministry of Education of Korea. This study was also supported by the Faculty of Civil Engineering, Ton Duc Thang University, Ho Chi Minh City and by the Faculty of Material Sciences, Ho Chi Minh University of Science HCMC, and VNU-HCMC, Viet Nam.

References

[1] T.D. Thanh, N.D. Chuong, H. Van Hien, T. Kshetri, L.H. Tuan, N.H. Kim, J.H. Lee, *Prog. Mater. Sci.,* **2018**, *96*, 51-85.

[2] T.D. Thanh, J. Balamurugan, H.V. Hien, N.H. Kim, J.H. Lee, *Biosens. Bioelectron*., **2017**, *96*, 186-193.

[3] J. Balamurugan, T.D. Thanh, N.H. Kim, J.H. Lee, *Biosens. Bioelectron*., **2016**, *83*, 68-76.

[4] K. Gopalsamy, J. Balamurugan, T.D. Thanh, N.H. Kim, D. Hui, J.H. Lee, *Compos. Part B Eng*., **2017**, *114*, 319-327.

[5] T.D. Thanh, N.D. Chuong, J. Balamurugan, H. Van Hien, N.H. Kim, J.H. Lee, *Small*, **2017**, *13(39)*, 1-11.

[6] T.D. Thanh, N.D. Chuong, H. Van Hien, N.H. Kim, J.H. Lee, *ACS Appl. Mater. Interfaces*, **2018**, *10(5),* 4672-4681.

[7] Y. Li, Y. Zhong, Y. Zhang, W. Weng, S. Li, Sensors Actuators, *B Chem*., **2015**, *206,* 735-743.

[8] X. Li, L. Zhi, *Chem. Soc. Rev*., **2018**, *47(9)*, 3189-3216.

[9] M.S. Artiles, C.S. Rout, T.S. Fisher, *Adv. Drug Deliv. Rev.,* **2011**, *63(14-15),* 1352-1360.

[10] S.K. Vashist, J.H.T. Luong, *Carbon*, **2015**, *84*, 519-550.

[11] B.. Hvolbæk, T.V.W.. Janssens, B.S.. J.K.. Nørskov, Catalytic activity of Au nanoparticles, *Nano Today*, **2007**, *2(4)*, 14-18.

[12] D.T. Thompson, *Nano Today*, **2007**, *2(4)*, 40-43.

[13] P. Priecel, H.A. Salami, R.H. Padilla, Z. Zhong, J.A. Lopez-Sanchez, *Cuihua Xuebao/Chinese J. Catal.,* **2016,** *37(10),* 1619-1650.

[14] R. Ciriminna, E. Falletta, C. Della Pina, J.H. Teles, M. Pagliaro, *Angew. Chemie - Int. Ed*., **2016**, *55(46)*, 14210-14217.

[15] S.H. Lim, E.-Y. Ahn, Y. Park, *Nanoscale Res. Lett.,* **2016***, 11(1)*, 474.

[16] Y. Li, H.J. Schluesener, S. Xu, *Gold Bull*. **2010**, *43(1)*, 29-41.

[17] S.M. Shawky, A.M. Awad, W. Allam, M.H. Alkordi, S.F. EL-Khamisy, *Biosens. Bioelectron*., **2017**, *92(15)*, 349-356.

[18] H. Aldewachi, T. Chalati, M.N. Woodroofe, N. Bricklebank, B. Sharrack, P.H. Gardiner, *Nanoscale*, **2017**, *10(1)*, 18-33.

[19] B.J. Lee, S.C. Cho, G.H. Jeong, *Curr. Appl. Phys*., **2015,** *15(5),* 563-568.

[20] T.D. Thanh, J. Balamurugan, S.H. Lee, N.H. Kim, J.H. Lee, *Biosens. Bioelectron*, **2016**, *81*, 259-267.

[21] M. Rybin, A. Pereyaslavtsev, T. Vasilieva, V. Myasnikov, I. Sokolov, A. Pavlova, E. Obraztsova, A. Khomich, V. Ralchenko, E. Obraztsova, *Carbon*, **2016**, *96*, 196-202.

[22] Z. Zafar, Z.H. Ni, X. Wu, Z.X. Shi, H.Y. Nan, J. Bai, L.T. Sun, *Carbon*, **2013**, *61*, 57-62.

[23] T.D. Thanh, J. Balamurugan, J.Y. Hwang, N.H. Kim, J.H. Lee, *Carbon*, **2016**, *98*, 90-98.

[24] T. Han, J. Jin, C. Wang, Y. Sun, Y. Zhang, Y. Liu, *Nanomaterials*, **2017**, *7*, 40.

[25] Y. Sim, J. Kwak, S.-Y. Kim, Y. Jo, S. Kim, S.Y. Kim, J.H. Kim, C.-S. Lee, J.H. Jo, S.-Y. Kwon, *J. Mater. Chem. A.*, **2018**, *6(4)*, 1504-1512.

[26] W. Wang, S. Guo, I. Lee, K. Ahmed, J. Zhong, Z. Favors, F. Zaera, M. Ozkan, C.S. Ozkan, *Sci. Rep*., **2014**, *4*, 9-14.

[27] X. Wang, X. Guo, J. Chen, C. Ge, H. Zhang, Y. Liu, L. Zhao, Y. Zhang, Z. Wang, L. Sun, *J. Mater. Sci. Technol*., **2017**, *33(3)*, 246-250.

[28] G. Zhu, Z. He, J. Chen, J. Zhao, X. Feng, Y. Ma, Q. Fan, L. Wang, W. Huang, *Nanoscale*., **2014**, *6(2)*, 1079-1085.

[29] T.D. Thanh, J. Balamurugan, N.T. Tuan, H. Jeong, S.H. Lee, N.H. Kim, J.H. Lee, *Biosens. Bioelectron*., **2017**, *89(2)*, 750-757.

[30] W. Choi, M.A. Shehzad, S. Park, Y. Seo, *RSC Adv*., **2017**, *7(12)*, 6943-6949.

[31] R. Blume, P.R. Kidambi, B.C. Bayer, R.S. Weatherup, Z.J. Wang, G. Weinberg, M.G. Willinger, M. Greiner, S. Hofmann, A. Knop-Gericke, R. Schlögl, *Phys. Chem. Chem. Phys*., **2014**, *16(47)*, 25989-26003.

[32] T. Li, J.A. Yarmoff, *Surf. Sci*., **2018**, *675*, 70-77.

[33] L.C. Wang, Y. Zhong, H. Jin, D. Widmann, J. Weissmüller, R.J. Behm, *Beilstein J. Nanotechnol*., **2013**, *4*, 111-128.

[34] M. Taei, E. Havakeshian, H. Salavati, F. Abedi, *RSC Adv.*, **2016**, *6(33)*, 27293-27300.

[35] W. Liu, X. Wu, X. Li, *RSC Adv*., **2017**, *7(58)*, 36744-36749.

[36] L. Yang, Y. Zhang, M. Chu, W. Deng, Y. Tan, M. Ma, X. Su, Q. Xie, S. Yao, *Biosens. Bioelectron*, **2014**, *52*, 105-110.

[37] J. Wang, H. Gao, F. Sun, C. Xu, *Sensors Actuators, B Chem.*, **2014**, *191*, 612-618.

[38] M. Liu, R. Liu, W. Chen, *Biosens. Bioelectron*., **2013**, *45*, 206-212.

[39] A. Weremfo, S.T.C. Fong, A. Khan, D.B. Hibbert, C. Zhao, *Electrochim. Acta.*, **2017**, *231*, 20-26.

[40] T. Kangkamano, A. Numnuam, W. Limbut, P. Kanatharana, P. Thavarungkul, *Sensors Actuators, B Chem*. **2017**, *246*, 854-863.

[41] D. Geng, X. Bo, L. Guo, *Sensors Actuators, B Chem*., **2017**, *244*, 131-141.